

## Direct Imaging of Dynamical Heterogeneities near the Colloid-Gel Transition

Y. Gao and M. L. Kilfoil\*

*Department of Physics, McGill University, Montréal, Canada H3A 2T8*

(Received 30 October 2006; published 15 August 2007)

We observe the microscopic dynamics of a suspension of colloids with attractive interaction by confocal fluorescence microscopy to provide a deeper understanding of the relationship between local structure and dynamics near the gel transition. We study the distinct and self-parts of the van Hove density-density correlation function applied to our experimental data. Separable fast and slow populations emerge in the self-part, while the distinct part shows a pronounced signature of dynamic heterogeneities close to the gel transition, dominated by the fast particles. The slow population close to the gel transition shares features with an attraction-driven colloidal glass, including a plateau in the mean squared displacement that provides an estimate for the dynamical localization length.

DOI: [10.1103/PhysRevLett.99.078301](https://doi.org/10.1103/PhysRevLett.99.078301)

PACS numbers: 82.70.Dd, 64.70.Pf, 82.70.Gg

Dynamical heterogeneity occurs when the particle mobilities in a system show diversity in different regions: the particles in some regions are mobile and in others are frozen. Dynamical heterogeneity is believed to be the origin of the slow structural relaxations that take place in molecular glasses and in model systems such as colloidal glasses and gels. In hard sphere liquids close to the glass transition, structural relaxation has been shown to take place through highly correlated stringlike motion of a few mobile particles [1,2]. The dynamical heterogeneity was found to be related to heterogeneity in the local density [2]. Recent molecular dynamics simulations near a gel transition show two distinct populations of particles with different mobilities, the “slow” particles forming a rigid network of particles, with the “fast” particles on the surface of the network where they tend to replace one another [3]. Despite the recent shift in paradigm that gels and glasses may be related in their dynamical behavior [4], there has been no direct measurement of the dynamical heterogeneity in colloidal gels.

Colloids can be prepared in nonequilibrium solid phases via a number of routes. Sudden crowding of hard spheres beyond a density, parametrized by volume fraction  $\phi$ , of  $\phi = 0.58$  produces a colloidal glass in which the individual particle dynamics become almost completely arrested. Adding nonadsorbing polymer into a noninteracting hard sphere system induces a short-range depletion attraction [5], parametrized by interaction strength  $U$ , that plays the role of inverse temperature [6]. Colloidal gelation occurs when a short-range attraction of sufficient strength  $U$  is induced between colloidal particles to form a sample-spanning network. As in glasses, rearrangement almost completely stops on solidification in gels, but at lower  $\phi$ .

There is mounting evidence that the different pathways to solidification brought about by crowding in hard spheres and by interparticle attraction in attractive systems might all be due to increased steric hindrance followed by glassy behavior at the onset of solidification. Evidence for such similar physics first came in the form of experimental verification [7] of reentrant behavior predicted by mode cou-

pling theory (MCT) [8] between a repulsive (hard sphere) glass and an attractive glass, amidst a large and growing number of studies [9] since the attraction-driven glass was first predicted. Recent light scattering experiments show that colloidal systems that form a gel by phase separating into colloid-rich and colloid-poor regions in fact solidify via a glasslike transition within the colloid-rich phase [10]. In a similar region of the  $(U, \phi)$  phase space, molecular dynamics simulations close to gelation show nonhomogeneous microscopic dynamics [3]. Experimental investigation of the microscopic dynamics is essential for guidance for a theoretical description of the dynamical arrest upon gelation and its relation to solidification in glasses.

In this Letter, we show the first direct observation of dynamical heterogeneities in colloidal gels. We study the three-dimensional structures formed at a low-to-moderate  $U$  by confocal fluorescence microscopy at controlled time intervals during the approach to colloidal gelation. We calculate the dynamics of our experimental data using the van Hove space-time correlation function.

The route to gelation we use is a fast quench upon mixing of the colloids and polymer, and a slow quench along a line in the phase diagram of increasing  $\phi$  and constant  $U$  [11] during which we perform experiments at different  $\phi$ , as depicted in Fig. 1. The relative buoyancy of the colloids is  $\Delta\rho = 0.011 \text{ g/cm}^3$ , corresponding to a gravitational height of  $h = k_B T / (4/3\pi a^3 \Delta\rho g) \sim 40$  particle radii  $a$ , where  $g$  is the acceleration due to gravity. Because the microscopic rearrangements we observe are local and we use interaction strengths  $U > k_B T$ , computed using approximated ideal solvent polymer radius of gyration and adjusted for the starting  $\phi$  [12], the gravitational field provides a slow densification while the interaction strength and steric hindrance govern the microscopic dynamics. In this Letter we present data for a sample at a low-to-moderate interaction strength of  $U = 2.86k_B T$ . In the Fig. 1 inset we show that  $\phi$  increases slowly, approaching  $\phi_G = 0.442$  following a power law  $(\phi_G - \phi) \sim t^{-3/2}$ .

The colloidal particles are 1.33- $\mu\text{m}$ -diam polymethylmethacrylate (PMMA) spheres, sterically stabilized by

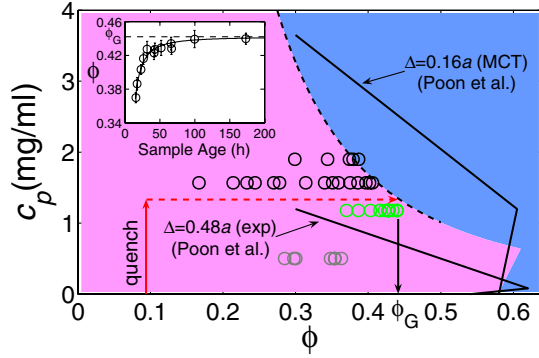


FIG. 1 (color online). The  $(\phi - c_p)$  phase space for colloidal gels and glasses, where polymer concentration  $c_p$  sets the attractive strength  $U$ , and  $R_g$  relative to  $a$  sets the range  $\Delta$ . Solid black lines are known dynamical arrest transition lines, obtained by MCT for  $\Delta = 0.16a$  [12] and by experiment for  $\Delta = 0.48a$  [7], that delimit our  $\Delta = 0.28a$  system. Dashed black line is roughly the phase boundary based on the arrest of structural relaxation over time scales of hours, for three different samples. Gray (red) arrows indicate the quenching strategy used. Experiments performed at different points along the route to gelation at a low-to-moderate interaction strength of  $U = 2.86k_B T$  are represented in light gray (green) symbols. Inset:  $\phi$  during approach to gelation. The solid line is a power law fit of the data,  $\phi = 0.442 - 5.09 \times t^{-1.56}$ .

chemically grafted poly-12-hydroxystearic acid, dyed with the electrically neutral fluorophore 4-chloro-7-nitrobenzo-2-oxa-1,3-diazole (NBD), and suspended in a solvent mixture of decahydronaphthalene (decalin), tetrahydronaphthalene (tetralin), and cyclohexyl bromide (CXB) that allows for independent matching of the refractive index and buoyancy of the particles. Polystyrene polymer (molecular weight 11 700 000 g/mol) is added at 1.177 mg/ml to induce a depletion attraction at a range estimated by  $\Delta = 2R_g = 0.28a$ , where  $R_g$  is the polymer radius of gyration. We collect stacks of images at fixed time intervals ranging from 12 to 1500 s at different  $\phi$  to access short and long time dynamics during the approach to gelation. From the stacks of images we extract the particle positions of 1000 particles in three dimensions and track their positions [14] at better than 10 nm resolution over time to use as input for the microscopic dynamics. We show an image and a 3-dimensional rendering from a stack of images at  $\phi = 0.429$  in Fig. 2(a) and 2(b).

We implement the van Hove space-time correlation function,  $G_d(r, \tau)$ , as

$$G_d(r, \tau) = \left\langle \frac{1}{\rho(t+\tau)N_{in}(t)} \times \sum_i^{N_{in}(t)} \sum_{j \neq i}^{N(t+\tau)} \delta(r - |\vec{r}_i(t) - \vec{r}_j(t+\tau)|) \right\rangle_t$$

for our experiment, with normalization factors  $N_{in}(t)$  equal to the number of particles within a subvolume [see Fig. 2(b)] to allow for computation of the pair correlation

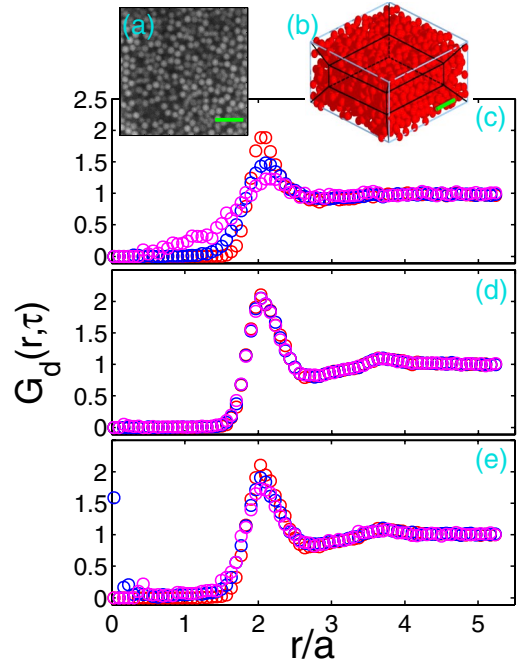


FIG. 2 (color online). Dynamical arrest during colloidal gelation for  $U/k_B T = 2.86$ . (a) Image from a stack at  $\phi = 0.429$ . The full volume section at each  $\phi$  is  $(22.6 \times 22.6 \times 10) \mu\text{m}^3$  at 200 nm spacing in  $z$ . Scale bar represents  $5 \mu\text{m}$ . (b) Geometry for calculation of the pair correlation function. (c)–(e) Distinct part of the van Hove correlation function. Dark gray (red), black (blue), and light gray (magenta) symbols represent (c)  $\tau = 0, 60, 480$  s for  $\phi = 0.37$ , (d)  $\tau = 0, 960, 2880$  s for  $\phi = 0.429$ , and (e)  $\tau = 0, 19200, 38400$  s for  $\phi = 0.429$ .

function to pair distances of  $5.2a$ , and  $\rho(t+\tau)$  equal to the number density for all the particles in the full volume. The average is performed over the time series since we ensure that each experiment is short relative to the sample age. At  $\tau = 0$  this function is the pair correlation function  $g(r)$ . For a fluid of noninteracting hard spheres,  $G_d(r, \tau \rightarrow \infty) = 1$  at all  $r$ . Structural arrest will result in arrest of  $G_d(r, \tau)$ .

We plot in Fig. 2 the correlation function  $G_d(r, \tau)$  at two different  $\phi$  en route to gelation. At  $\phi = 0.37$  [Fig. 2(c)], the structure decays on time scales from 0 to 8 min. At  $\phi = 0.429$  [Fig. 2(d)], the distinct correlation is completely frozen over similar time scales. At  $\tau$  of up to 11 h at  $\phi = 0.429$  [Fig. 2(e)], the peak at the shell of nearest neighbors decays only slightly, yet dramatically different behavior appears in a peak at  $r = 0$ . This latter is a signature of some particle motions into positions previously occupied by other particles. Remarkably, this behavior in  $G_d(r, \tau)$  close to gelation is in near perfect agreement with that observed in molecular dynamics simulations using parameters chosen to model colloids with a depletion attraction of range similar to that presented in this Letter, despite the deeper potential well of the simulated system [3].

We plot the ensemble-averaged mean squared displacement in the approach to gelation in Fig. 3. Far from the transition we observe nearly diffusive behavior. As  $\phi$  increases to  $\phi \sim 0.43$ , the time scale for  $\langle \Delta r^2 \rangle$  to reach

$0.2a^2$ , an arbitrary measure of time scale for relaxation, increases by more than 3 orders of magnitude. This time scale, reported in the inset of Fig. 3, increases as a power law with  $(\phi_G - \phi)$  close to the gel transition.

To further elucidate the microscopic dynamics, we plot the self part of the van Hove correlation function  $G_s(x, \tau)$  defined as  $G_s(x, \tau) = (1/N) \sum_{i=1}^N \delta[x + x_i(0) - x_i(\tau)]$ , the probability distribution of displacements of the tracked particles at time  $\tau$  [15]. Figure 4 shows the 1-dimensional distribution  $G_s(x, \tau)$  for  $\phi = 0.429$  at different lag times, compared with the Gaussian form expected for a liquid [16]. We observe significant deviation of the distributions from Gaussian at all  $\tau$ . At long lag times two distinct Gaussian distributions emerge in  $G_s(x, \tau)$ , across all  $\phi$  we study. We fit the  $G_s(x, \tau)$  to a bimodal Gaussian form, assigning the broad and narrow Gaussian widths  $\sigma_1$  and  $\sigma_2$  over all  $\tau$ , shown in the inset of Fig. 4(c) for  $\phi = 0.429$ . Using this method we estimate the fractions of mobile and immobile particles at each  $\phi$ . We find that the slow population grows at the expense of the fast population on the approach to the gelation transition [17].

We identify fast and slow particles independently at each  $\phi$  by defining a mobility for each particle based on its average magnitude of displacement during each time step  $\delta t$ ,  $\langle |\vec{r}(t + \delta t) - \vec{r}(t)| \rangle_t$ , rank order the particles according to this mobility, and select the subset of those fastest and slowest particles such that the Gaussian widths of the  $G_s(x, \tau)$  of the resulting subpopulations match  $\sigma_1$  and  $\sigma_2$  over long lag times. This method allows us to identify the actual populations of mobile and immobile particles at each  $\phi$ . The distribution  $G_s(x, \tau = 41\,280\text{ s})$  of the mobile population for  $\phi = 0.429$  is superimposed in Fig. 4(c), and completely reproduces the fast component obtained from the two-Gaussian fit.

We plot the distinct van Hove correlation function for the fast and slow populations separately for  $\phi = 0.440$ , very near the gelation transition, in Fig. 5. The correlation functions show clearly that the fast particles alone (at the

bottom) account for nearly all of the long-time-scale rearrangements near  $r = 0$ . These correlations provide emphatic justification for the extraction of fast and slow populations from the self-van Hove functions. At right in Fig. 5 we show the microscopic configuration of these fast and slow populations. The immobile particles appear to be interconnected. The fast particles do not form a network, evidently moving as single particles or clusters.

We plot the mean squared displacements of the slow and fast populations in the insets of Fig. 5. The slow particle mean-square displacement (MSD) lies well below and the fast particle MSD well above the all-particle mean-square displacement at all  $\tau$ , confirming that the fast particles dominate the dynamics close to the transition. The localization length is manifested as a plateau in the mean-square displacement of the slow particles at  $\sim 0.076a^2 \approx \Delta^2$ , a height comparable to the plateau height of order  $\Delta^2$  observed in simulations [7,18] close to the attractive glass. For the range of interaction investigated, this length scale estimate is in simultaneous agreement with both ‘‘caging’’ due to crowding, at  $\sim 0.2a$  [7,18,19], and a cage formed by the potential well. It remains to be seen whether the two

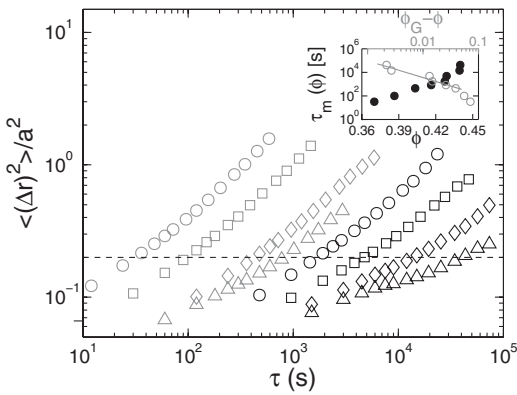


FIG. 3. Particle mean squared displacements  $\langle \Delta r^2(\tau) \rangle / a^2$  plotted versus lag time at, left to right,  $\phi = 0.37, 0.386, 0.403, 0.416, 0.427, 0.428, 0.439, 0.440$ . Inset: Dependence of the time  $\tau$  when  $\langle \Delta r^2 \rangle = 0.2a^2$  on  $\phi$  (closed symbols, bottom axis) and on  $\phi_G - \phi$  (open symbols, top axis).

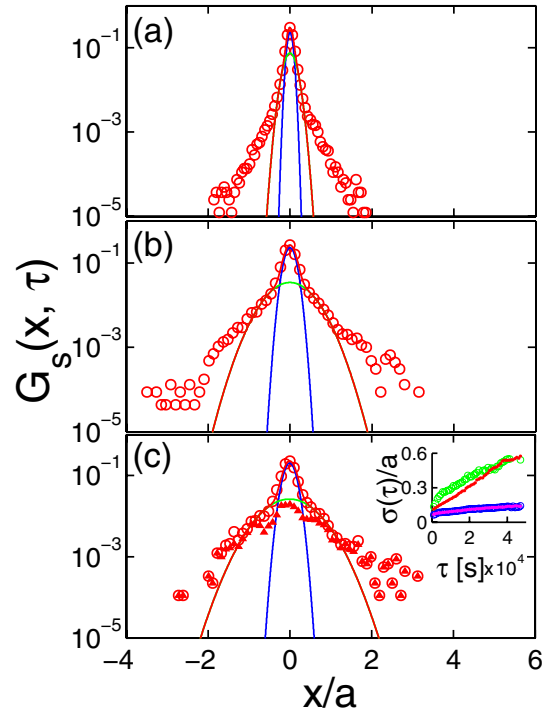


FIG. 4 (color online). Bimodal Gaussian fits [dark gray (red) solid lines] to  $G_s(x, \tau)$  at  $\phi = 0.429$  and  $\tau = 960\text{ s}$  (a),  $31\,680\text{ s}$  (b), and  $41\,280\text{ s}$  (c). Light gray (green) and black (blue) lines indicate the fast and slow branches. Inset: Broad [light (green) symbols] and narrow [dark (blue) symbols] widths obtained from the bimodal Gaussian fits to  $G_s(x, \tau)$ . Widths of Gaussian fits to  $G_s(x, \tau)$  for fast [dark (red) line] and slow [light (magenta) line] populations alone identified based on single-particle average displacements are also shown in the inset. The distribution  $G_s(x, \tau = 41\,280\text{ s})$  of the subpopulation of fast particles is plotted as solid symbols in (c).

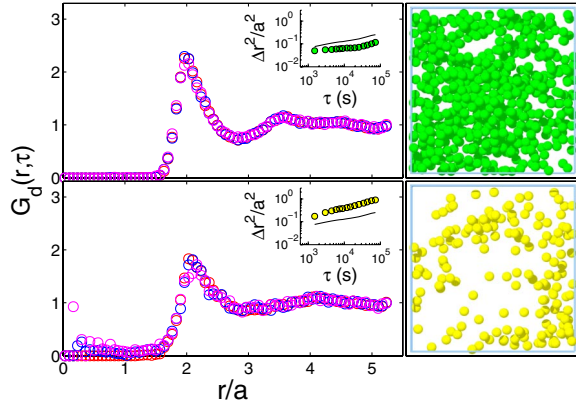


FIG. 5 (color online). Top:  $G_d(r, \tau)$  for the population of 550 slow particles separately at  $\phi = 0.440$ . Dark gray (red), black (blue), and light gray (magenta) symbols represent  $\tau = 0, 30\,000$ , and  $55\,500$  s, respectively. Inset:  $\langle \Delta r^2 \rangle_{\text{slow}}(\tau)$  (symbols), with  $\langle \Delta r^2 \rangle_{\text{all}}(\tau)$  as solid line. Bottom:  $G_d(r, \tau)$  for the 250 fast particles. Inset:  $\langle \Delta r^2 \rangle_{\text{fast}}(\tau)$  in (yellow) symbols. At right: Renderings of slow (top) and fast (bottom) particles at  $\phi = 0.440$ .

types of mechanisms constraining the particle motion are distinguishable via confocal fluorescence microscopy in a colloidal system with range of potential  $\Delta \ll 0.2a$ .

This work reveals separable fast and slow components in the microscopic dynamics of a colloidal system close to gelation. The slow particles seemingly form a backbone whose structure barely relaxes on any microscopic length scales. This microscopic picture is complementary to that obtained from light scattering experiments and mode coupling theory that gelation in some systems is driven by a local arrest of the dynamics. The slow particles show dynamical behavior reminiscent of glasses obtained by the volume fraction route, lending support to the idea that these systems can be considered under the same conceptual framework. There are nevertheless important differences observed: separable fast and slow components are not observed in hard sphere glasses, most likely because the mobile regions in gels tend to nucleate around the voids that are a unique part of their structure. The distinct part of the van Hove correlation function has never been measured experimentally in glasses obtained by the volume fraction route.

There are many possible routes to gelation. The results presented in this Letter describe the microscopic dynamics along the  $\phi$  pathway to gelation. There is surprising agreement with the simulated microscopic dynamics along the  $U$  pathway to gelation at similar range of interaction [3] but deeper potential well. These results can serve as a standard description of microscopic dynamics to compare to other possible routes to colloidal gelation.

We thank Andrew Schofield and Peter Pusey of University of Edinburgh for providing PMMA latex particles. This work was supported by the Canadian Foundation for Innovation (CFI) and the Natural Sciences and Engineering Research Council of Canada (NSERC).

\*kilfoil@physics.mcgill.ca

- [1] C. Donati, S. C. Glotzer, P. H. Poole, W. Kob, and S. J. Plimpton, *Phys. Rev. E* **60**, 3107 (1999).
- [2] E. R. Weeks, J. C. Crocker, A. C. Levitt, A. Schofield, and D. A. Weitz, *Science* **287**, 627 (2000).
- [3] A. M. Puertas, M. Fuchs, and M. E. Cates, *J. Chem. Phys.* **121**, 2813 (2004); A. M. Puertas, M. Fuchs, and M. E. Cates, *J. Phys. Chem. B* **109**, 6666 (2005).
- [4] K. Dawson, *Curr. Opin. Colloid Interface Sci.* **7**, 218 (2002); F. Sciortino, *Nat. Mater.* **1**, 145 (2002).
- [5] S. Asakura and F. Oosawa, *J. Chem. Phys.* **22**, 1255 (1954).
- [6] A. Liu and S. Nagel, *Nature (London)* **396**, 21 (1998); V. Trappe, V. Prasad, L. Cipelletti, P. N. Segre, and D. A. Weitz, *Nature (London)* **411**, 772 (2001).
- [7] K. N. Pham, A. M. Puertas, J. Bergenholtz, S. Egelhaaf, A. Moussaid, P. N. Pusey, A. B. Schofield, M. E. Cates, M. Fuchs, and W. C. K. Poon, *Science* **296**, 104 (2002).
- [8] J. Bergenholtz and M. Fuchs, *Phys. Rev. E* **59**, 5706 (1999); L. Fabbian, W. Götze, F. Sciortino, P. Tartaglia, and F. Thery, *Phys. Rev. E* **59**, R1347 (1999).
- [9] E. Zaccarelli, I. Saika-Voivod, S. Buldyrev, A. Moreno, P. Tartaglia, and F. Sciortino, *J. Chem. Phys.* **124**, 124908 (2006); K. Dawson, G. Foffi, M. Fuchs, W. Götze, F. Sciortino, M. Sperl, P. Tartaglia, T. Voigtmann, and E. Zaccarelli, *Phys. Rev. E* **63**, 011401 (2000); M. Sztucki, T. Narayanan, G. Belina, A. Moussaid, F. Pignon, and H. Hoekstra, *Phys. Rev. E* **74**, 051504 (2006).
- [10] S. Manley, H. M. Wyss, K. Miyazaki, J. C. Conrad, V. Trappe, L. J. Kaufman, D. R. Reichman, and D. A. Weitz, *Phys. Rev. Lett.* **95**, 238302 (2005).
- [11] This implies polymer concentration is uniform and constant during gravity-induced solidification. The large asymmetry between polymer coil diffusion time  $\sim 0.3$  s and particle sedimentation time  $\sim 260$  s over one particle diameter at this  $\Delta\rho$  should assure polymer uniformity. The correction to reservoir polymer concentration due to the presence and configuration of colloids according to  $n_p^{(R)} = n_p/\alpha$  [12,13] for initial volume fraction of 0.1 changes by  $<1\%$  as solidification proceeds to  $\phi = 0.440$  in the colloid-rich region. Hence  $U$  may be safely assumed to be constant.
- [12] S. M. Ilett, A. Orrock, W. C. K. Poon, and P. N. Pusey, *Phys. Rev. E* **51**, 1344 (1995).
- [13] H. N. W. Lekkerkerker, *Colloids Surf.* **51**, 419 (1990).
- [14] J. C. Crocker and D. G. Grier, *J. Colloid Interface Sci.* **179**, 298 (1996).
- [15] A. Rahman, *Phys. Rev.* **136**, A405 (1964).
- [16] J. M. Haile, *Molecular Dynamics Simulation: Elementary Methods* (Wiley InterScience, New York, 1997).
- [17] See EPAPS Document No. E-PRLTAO-99-019731 for a supplementary figure showing the fractions of mobile and immobile populations as a function of  $\phi$  obtained via the method shown in Fig. 4. For more information on EPAPS, see <http://www.aip.org/pubservs/epaps.html>.
- [18] A. M. Puertas, M. Fuchs, and M. E. Cates, *Phys. Rev. E* **67**, 031406 (2003).
- [19] E. R. Weeks and D. A. Weitz, *Phys. Rev. Lett.* **89**, 095704 (2002).